Properties of Cosmic Deuterons Measured by the Alpha Magnetic Spectrometer SUPPLEMENTAL MATERIAL

For references see the main text.

Detector.—AMS is a general purpose high-energy particle physics detector in space. The layout of the detector is shown in Fig. S1. The main elements are the permanent magnet, the silicon tracker, four planes of time of flight (TOF) scintillation counters, the array of anticoincidence counters (ACCs), a transition radiation detector (TRD), a ring imaging Čerenkov detector (RICH), and an electromagnetic calorimeter (ECAL).

The AMS coordinate system is concentric with the magnet. The x axis is parallel to the main component of the magnetic field and the z axis points vertically with $z = 0$ at the center of the magnet. The (y-z) plane is the bending plane. Above, below, and downward-going refer to the AMS coordinate system. The central field of the magnet is 1.4 kG. Before flight, the field was measured in 120 000 locations to an accuracy of better than 2 G. On orbit, the magnet temperature varies from -3 to $+20$°C. The field strength is corrected with a measured temperature dependence of $-0.09\%/$°C.

The tracker has nine layers, the first ($L1$) at the top of the detector, the second ($L2$) just above the magnet, six ($L3$ to $L8$) within the bore of the magnet, and the last ($L9$) just above the ECAL. $L2$ to $L8$ constitute the inner tracker. Each layer contains double-sided silicon microstrip detectors that independently measure the x and y coordinates. The tracker accurately determines the trajectory of cosmic rays by multiple measurements of the coordinates with a resolution in each layer of 10 μm for $|Z|$=1 particles in the bending (y) direction. Together, the tracker and the magnet measure the rigidity of charged cosmic rays.

Each layer of the tracker provides an independent measurement of the charge number Z with a resolution of $\sigma_Z = 0.092$ for $Z = 1$ particles. Overall, the inner tracker has a resolution of $\sigma_Z = 0.049$ for $Z = 1$ particles.

Two TOF planes are located above the magnet (upper TOF) and two planes are below the magnet (lower TOF). The overall velocity ($\beta = v/c$) resolution has been measured to be $\sigma(1/\beta) = 0.04$ for $|Z|$=1 particles. The pulse heights of the two upper planes are combined to provide an independent measurement of the charge with accuracy $\sigma_Z = 0.06$ charge units for $|Z|$=1 particles. The pulse heights from the two lower planes are combined to provide another independent charge measurement with the same accuracy.

The RICH detector [27] measures the particle velocity and charge magnitude. It is located below the lower TOF and consists of two radiators, an expansion volume, and a photo-detection plane. The dielectric radiators induce the emission of a cone of Čerenkov photons when traversed by charged particles with a velocity greater than the velocity of light in the radiator. The central radiator is formed by sodium fluoride (RICH-NaF) of refractive index $n = 1.33$, it is surrounded by silica aerogel (RICH-Agl) of refractive index $n = 1.05$. This allows the detection of particles with velocities $\beta > 0.75$ for those that pass through the NaF radiator and $\beta > 0.952$ for those that pass through the Agl radiator. The expansion volume extends along z for 470 mm between the radiators and the photo-detection plane and it is surrounded by a high reflectivity mirror to increase detection efficiency. The photo-detection plane is an array of 10880 photosensors in multi-channel photomultiplier tubes with an effective spatial granularity of 8.5×8.5 mm^2. For $Z = 1$ particles, the RICH velocity resolution, σ_β, is 3.5×10^{-3} for NaF and 1.2×10^{-3} for Agl.

Deuterons traversing AMS were triggered as described in Ref. [32]. The trigger efficiency has been measured to be >83% over the entire rigidity range.

Monte Carlo simulated events were produced using a dedicated program developed by the collaboration based on the GEANT4-10.3 package [28]. The program simulates electromagnetic and hadronic interactions of particles in the material of AMS and generates

detector responses. The digitization of the signals is simulated precisely according to the measured characteristics of the electronics. The simulated events then undergo the same reconstruction as used for the data.

Event selection.— The collection time used in this analysis includes only those seconds during which the detector was in normal operating conditions and, in addition, AMS was pointing within 40° of the local zenith, and the International Space Station (ISS) was outside of the South Atlantic Anomaly. Because of the influence of the geomagnetic field, the collection time for Galactic cosmic rays increases with rigidity, reaching 2.2×10^8 seconds at 21 GV.

Deuterons are required to be downward going and to have a reconstructed track in the inner tracker which passes through $L1$. Charge measurements on $L1$, the upper TOF, the inner tracker, and the lower TOF are required to be compatible with $Z = 1$. Track fitting quality criteria such as a $\chi^2/\mathrm{DOF} < 10$ in the bending plane are applied.

The measured rigidity is required to be greater than a factor of 1.2 times the maximum geomagnetic cutoff within the AMS field of view. The cutoff was calculated by backtracing [29] from the top of AMS out to 50 Earth's radii using the most recent International Geomagnetic Reference Field model [30].

For events with a velocity above the Čerenkov thresholds, we require additional quality criteria such as the number of hits in the reconstructed Čerenkov ring ≥ 4, and compatible velocity measurements in the TOF and the RICH.

Background estimation.— The background to D comes overwhelmingly from the He fragmentation in the AMS materials, mainly C and Al, above $L1$. This background is estimated from data by measuring the relative branching ratios of the reactions $\mathrm{He} + (\mathrm{C}, \mathrm{Al}) \rightarrow \mathrm{D} + X$, $f_{\mathrm{He}\rightarrow\mathrm{D}}$, and $\mathrm{He} + (\mathrm{C}, \mathrm{Al}) \rightarrow \mathrm{T} + X$, $f_{\mathrm{He}\rightarrow\mathrm{T}}$, using nuclei with measured $Z = 2$ by $L1$ and measured $Z = 1$ by $L2$ to $L8$, see Fig. S2. Nuclei mass is measured from the combination of rigidity (R) measured by the Tracker and velocity (β) measured either by the TOF or the RICH, depending on the nuclei kinetic energy, using the formula $m = R\sqrt{1/\beta^2 - 1}$. Fits to data yield ratios $f_{\mathrm{He}\rightarrow\mathrm{D}}/f_{\mathrm{He}\rightarrow\mathrm{T}} = 1.0 - 1.4$ in the $0.5 - 10$ GeV/n kinetic energy range. The kinetic energy dependence of $f_{\mathrm{He}\rightarrow\mathrm{D}}/f_{\mathrm{He}\rightarrow\mathrm{T}}$ measured from data is modeled with a polynomial. After the event selection, the background on the measured number of D nuclei was calculated as $f_{\mathrm{He}\rightarrow\mathrm{D}}/f_{\mathrm{He}\rightarrow\mathrm{T}} \times N_i^T$, where N_i^T is the number of tritium nuclei measured in the ith rigidity bin, and then subtracted bin by bin. The corresponding relative correction of the measured number of D has been found to be 3.6±0.9% from 1.9 to 7 GV, decreasing to 2.1±0.2% at 21 GV, as shown in Fig. S3.

Unfolding procedure.— The fluxes of D are measured by unfolding the two-dimensional event distributions in rigidity (R) and velocity (β) of 200×200 bins. The rigidity resolution function, determined from MC simulations, has been extensively verified with the data [32]. The inverse velocity ($1/\beta$) resolution functions of the TOF and the RICH were first studied at $\beta \simeq 1$ with data, as shown in Fig. S4. The resolution functions were modeled as the sum of two Gaussians sharing the same mean value and an additional asymmetric Gaussian distribution, the latter to describe the tails in the reconstructed velocity. The dependence of the velocity resolution functions on β value was obtained from MC and compared with data, resulting in resolution functions relative corrections of $< 5\%$ over the entire rigidity range.

The number of events measured in ith bin in velocity and jth bin in rigidity, $\tilde{N}_{ij}$, includes contributions from cosmic p and D as well as the contributions from D and T produced by interactions of He above $L1$. The two-dimensional velocity and rigidity resolution functions,

in the form of migration matrices for the unfolded rigidity bin k, P_{ij}^k, D_{ij}^k, and I_{ij}^k for p, D, and T, respectively, are obtained from Monte Carlo simulations and verified with data. The number $\tilde{N}_{ij}$ is then given by

$$\tilde{N}_{ij} = \sum_k P_{ij}^k N_k^p + D_{ij}^k N_k^D + I_{ij}^k N_k^T \tag{S1}$$

where N_k^p, N_k^D, and N_k^T are the unfolded p, D, and T events with rigidity in bin k at the top of AMS.

The weighted Tikhonov regularization method was used to unfold the corresponding event numbers. This method minimizes the difference between data and the result of Eq. (S1) by computing a χ^2-like term with the additional regularization part, which damps irregular unfolding solutions. Specifically, the method employs a L^2-norm regularization term, and optimizes it by using the L-curve method [31]. To address variations in the detector response with rigidity inside each final bin, the unfolded results were obtained in the 200 rigidity bins, and the neighboring bins were merged together, to obtain the final 26 bins. The systematic error due to the unfolding procedure itself is obtained by changing the regularization weight until the χ^2-test agreement between Eq. (S1) and data decreases by 1σ. This procedure yields a systematic error of 1.7% below 6 GV, 1% from 6 to 8 GV, and 0.6% from 8 to 21 GV.

As an example of the power of the method to separate isotopes, Fig. S5 presents the rigidity unfolded p, D, and T two-dimensional distribution for $\beta > 0.952$, measured during one period of four Bartels rotations in 2016.

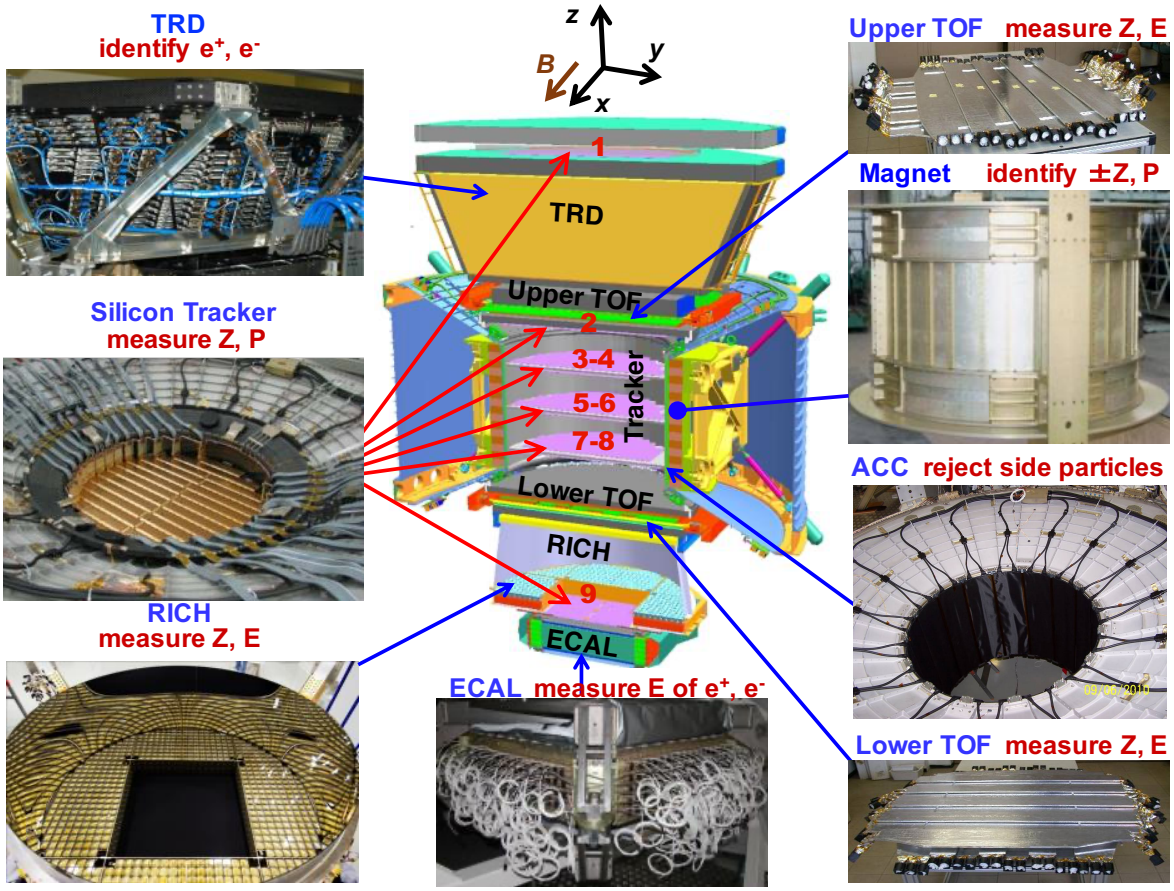

FIG. S1. The AMS detector, its main components and their functions. AMS is a TeV precision, multipurpose particle physics magnetic spectrometer in space. It identifies particles and nuclei by their charge number Z, energy E, and momentum P or rigidity ($R = Pc/Ze$), which are derived from redundant measurements by combinations of the Tracker, TOF, RICH, and ECAL. The ACC counters, located in the magnet bore, are used to reject particles entering AMS from the side. The AMS coordinate system is also shown. The x axis is parallel to the main component of the magnetic field and the z axis points vertically with $z = 0$ at the center of the magnet.

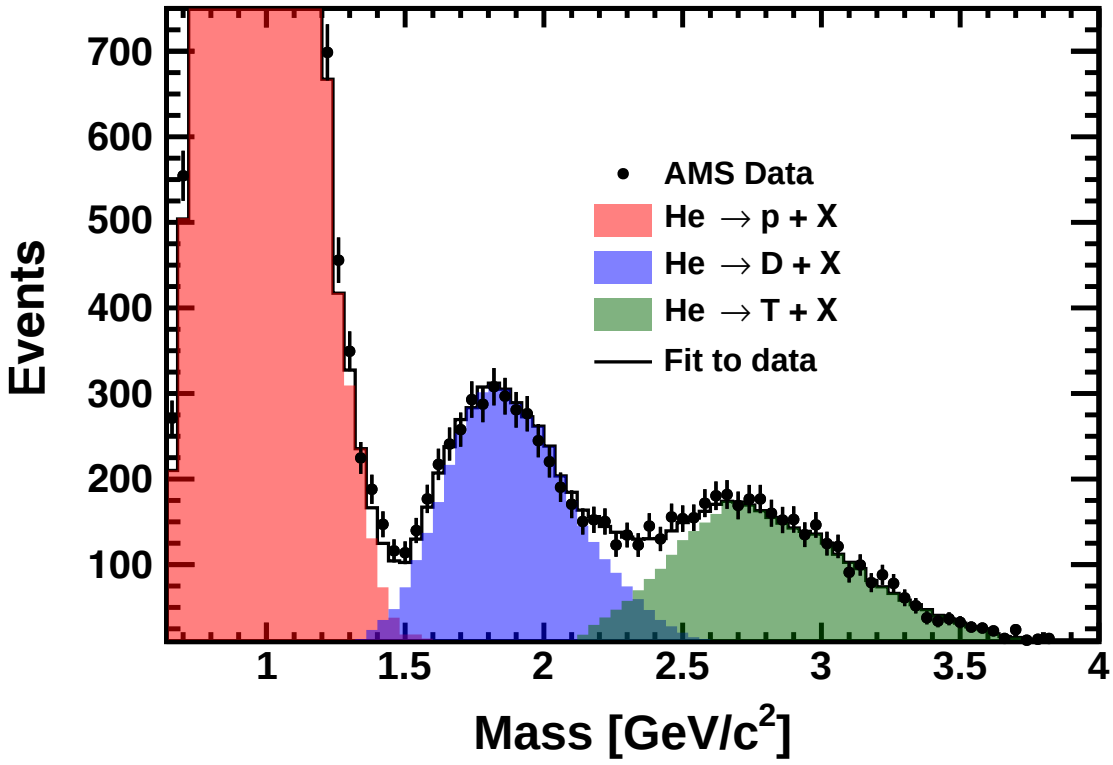

FIG. S2. Mass distribution of He events interacting between $L1$ and $L2$ with $0.6 < E_k < 0.75$ GeV/n for data (black points) and p, D and T mass templates (red, blue and green histograms, respectively) obtained from MC simulation. The black line shows the template fit to the data, yielding the ratio of $(\mathrm{He} \to \mathrm{D} + \mathrm{X})/(\mathrm{He} \to \mathrm{T} + \mathrm{X}) = 1.27 \pm 0.02$ for this particular kinetic energy bin. The events were selected by requiring a measured $Z = 2$ in tracker $L1$ and $Z = 1$ in the inner tracker ($L2$-$L8$).

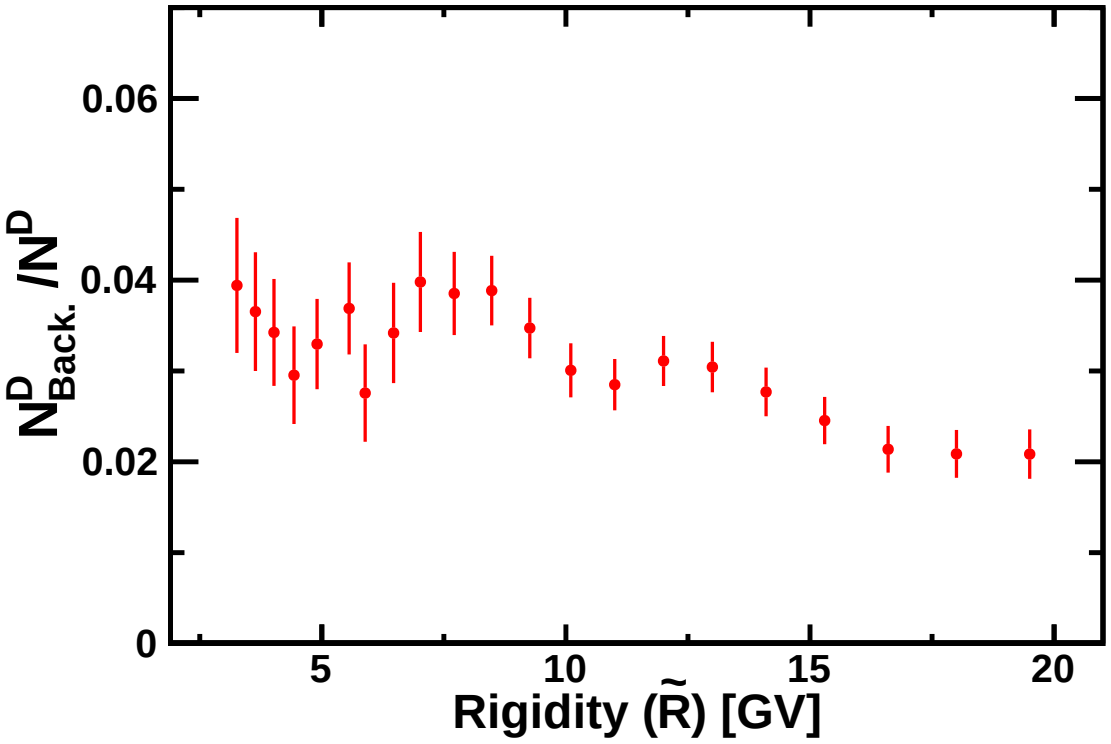

FIG. S3. Relative number of background ($N^{\mathrm{D}}_{\mathrm{Back.}}$) to the measured number of D (N^{D}) as a function of rigidity.

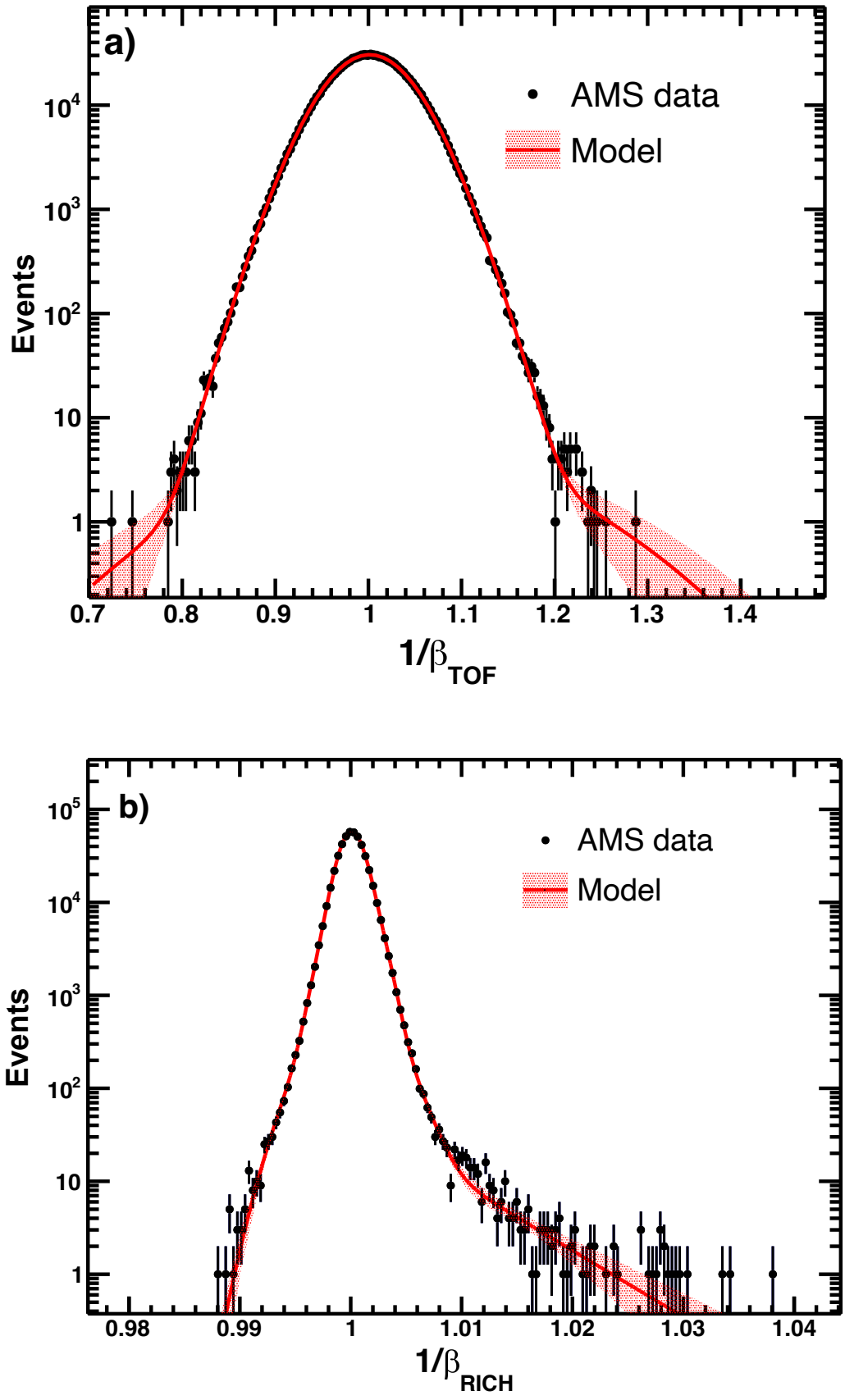

FIG. S4. Reconstructed inverse velocity ($1/\beta$) distributions at $\beta \simeq 1$ (50 GV$<$ R $<$200 GV) for $Z = 1$ events obtained using (a) the TOF and (b) the RICH. The distributions were modeled (solid red curves) as the sum of two Gaussians sharing the same mean value and an additional asymmetric Gaussian distribution. The red bands show the model uncertainty (2σ).

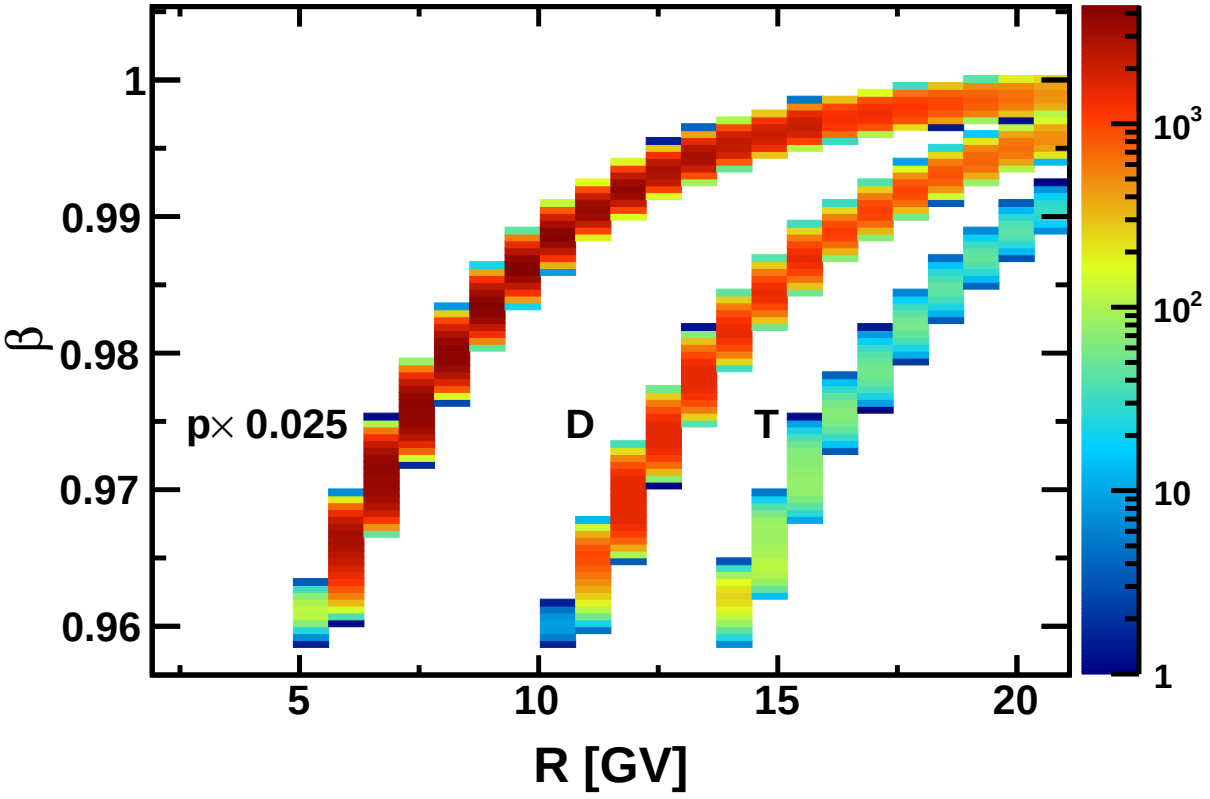

FIG. S5. Rigidity unfolded p, D, and T two-dimensional (β, R) event count distribution for $\beta > 0.952$, measured during one period of four Bartels rotations in 2016. Color indicates number of events, with p events scaled by 2.5×10^{-2}.

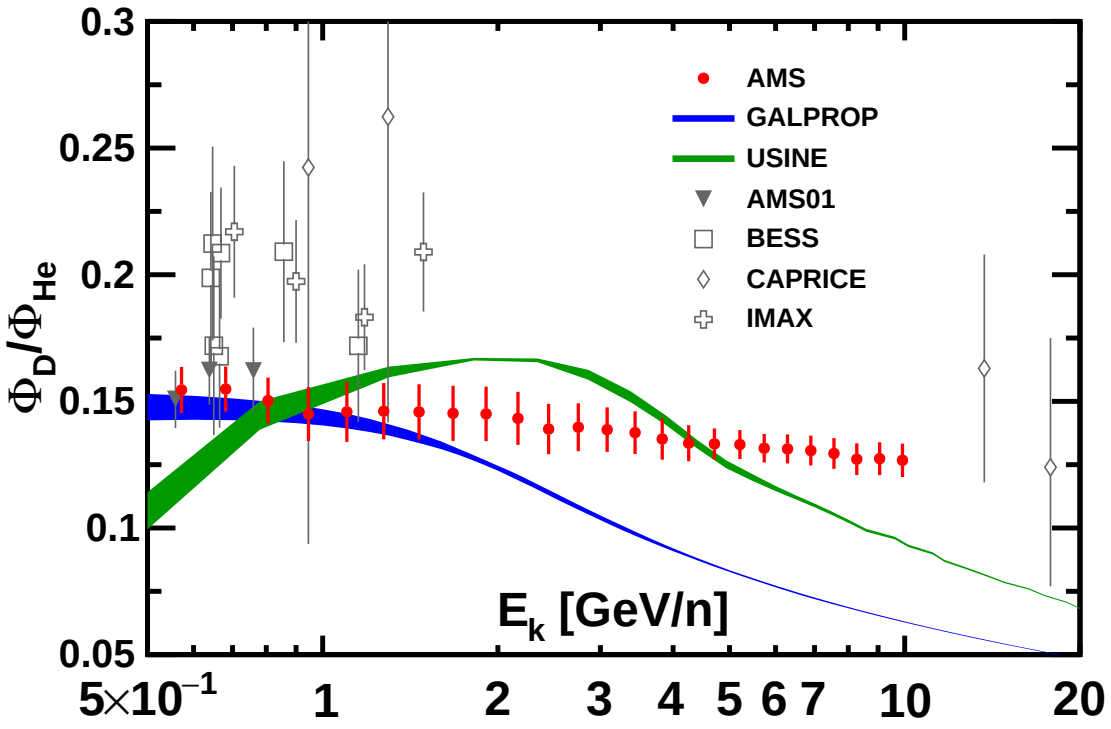

FIG. S6. The AMS D/He flux ratio as a function of kinetic energy per nucleon with total errors, together with previous measurements [13–16] and the predictions of the propagation models GALPROP [34] (blue shaded area) and USINE [35] (green shaded area). The shaded areas show the variations of the model predictions due to solar modulation. As seen, the AMS results on the D/He flux ratio disagree with the GALPROP predictions above ∼2 GeV/n and disagree with the USINE predictions from ∼1.5 to 3.5 GeV/n and above ∼5 GeV/n.

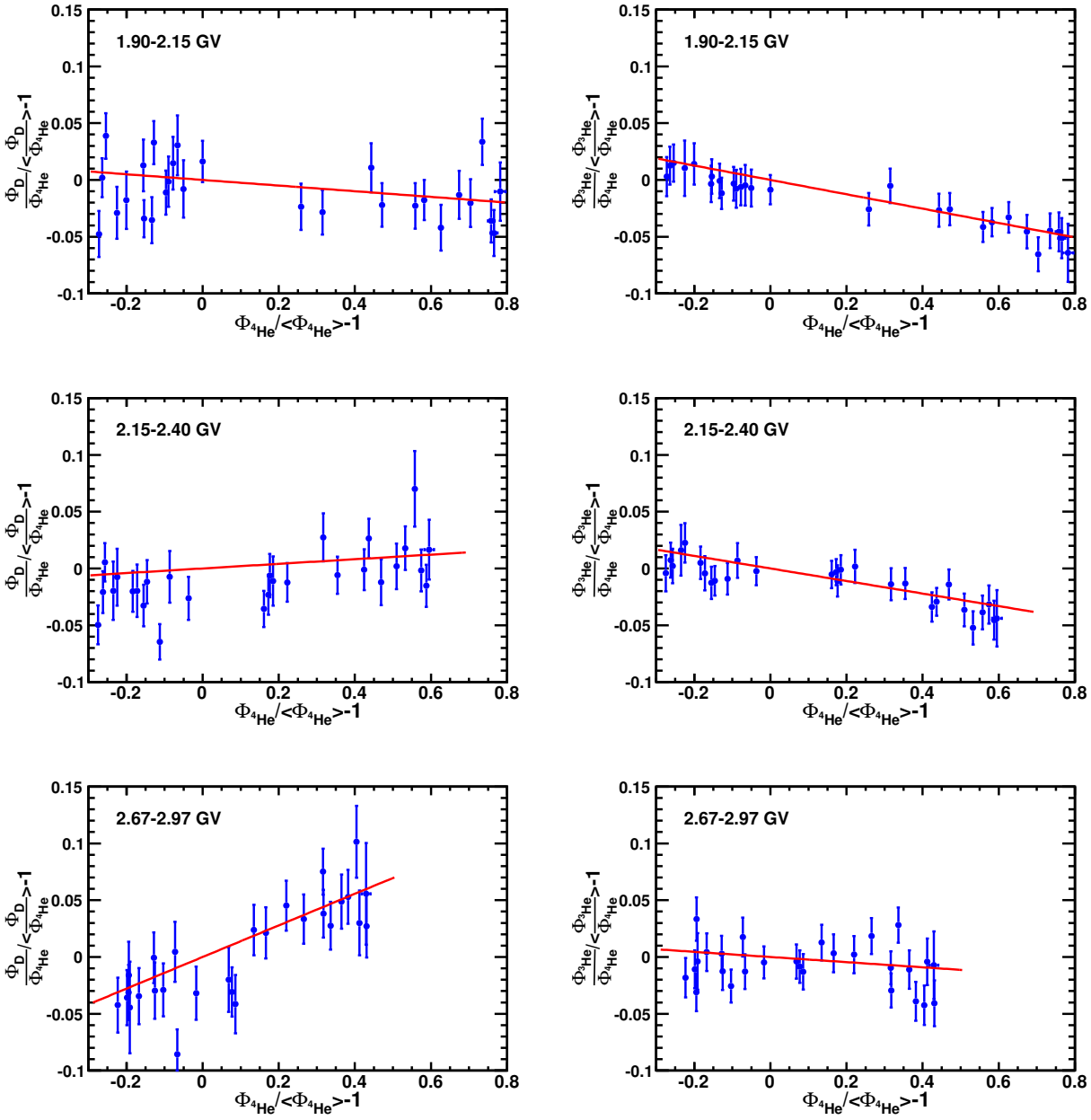

FIG. S7. The AMS D/^{4}He (left panels) and ^{3}He/^{4}He (right panels) flux ratios as functions of ^{4}He flux for three characteristic rigidity bins. The red lines show fit results with Eq. (2) and Eq. (3), to obtain slopes $k_{\rm D}$ and $k_{^3{\rm He}}$, respectively.

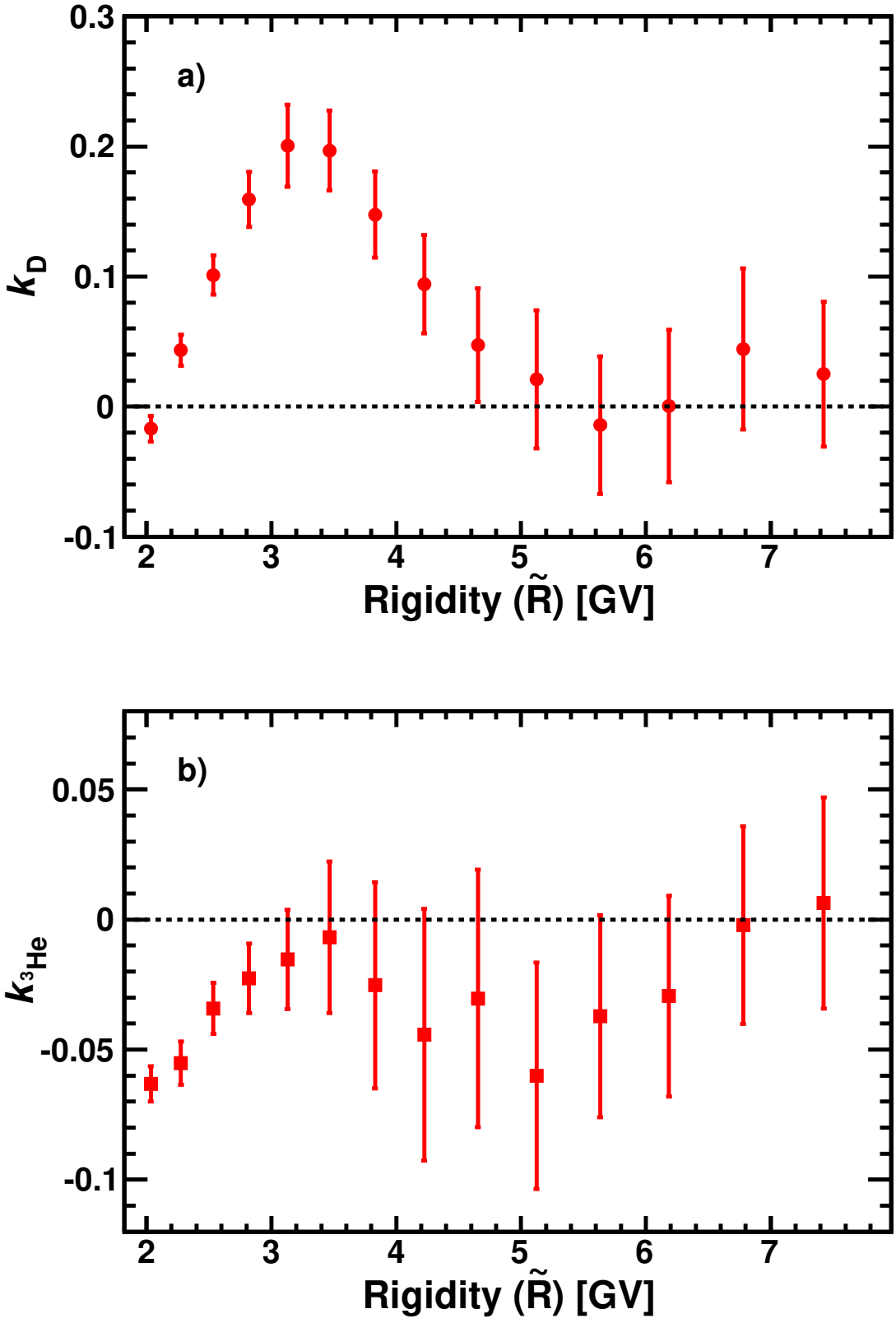

FIG. S8. Slopes, k fitted values for a) D/^{4}He with Eq. (2) and b) ^{3}He/^{4}He with Eq. (3) as functions of rigidity.